Supplementary Information

Structural and chemical mapping of Au-Co(OH)$_2$ electrocatalytic films shows the formation of ordered Au crystallites and the suppression of Co oxidation

Rusha Kamar,[a] Cameron M. Kewish,[b,c] David J. Paterson,[b] Tony Wang,[d] Anthony P. O'Mullane[a,†] and Michael M. W. Jones[a,d,†,*]

a. School of Chemistry and Physics, Queensland University of Technology (QUT), Brisbane, QLD 4001, Australia.
b. Australian Synchrotron, Australian Nuclear Science and Technology Organisation, Clayton, Victoria 3168, Australia.
c. Department of Chemistry and Physics, La Trobe Institute for Molecular Science, La Trobe University, Bundoora, Victoria 3086, Australia
d. Central Analytical Research Facility (CARF), Queensland University of Technology (QUT), Brisbane, QLD 4001, Australia.

Experimental Methods:

Sample preparation: Four films: Co pre, Co post, CoAu pre and CoAu post, were prepared on Si_3N_4 substrates that were previously coated with 2 nm Ti followed by 10 nm Pt by methods described previously[1], with the only exception in the electrodeposition time of 300 s. The electrodeposition time was longer to prepare thicker films for increased interaction volume of the films with incident X-ray to acquire better signals for XRD and XANES.

All electrochemical measurements were performed in a three-electrode set-up with a leak-free Ag/AgCl (3 M KCl) (e-DAQ) as the reference electrode due to its low sensitivity to oxygen and high stability in alkaline condition, and a Pt wire (BASi) as the counter electrode using a Biologic VSP potentiostat. A glassy carbon electrode (BASi) with 3 mm diameter was used as the working electrode. The deposition potential applied was -1.05 V vs Ag/AgCl for both films and the OER potential applied for the chronoamperometric experiments was 0.75 V vs Ag/AgCl for 4 h. 0.1 M NaOH was used as the electrolyte for the OER. Electrochemical impedance spectroscopy (EIS) was carried out over a frequency range of 1 MHz to 1 mHz with an amplitude of 10 mV. Cyclic voltammetry experiments to determine OER performance of both films were performed at a scan rate of 20 mVs^{-1}. A Pt coated Si wafer was tested for any OER activity in the scan range of 0.9 – 1.96 V (vs RHE) at a sweep rate of 20 mVs^{-1} in 0.1 M NaOH to rule out any influence from the underlying Pt/Si layer in the potential region of interest.

All electrolytes and deposition solution were prepared with Milli-Q water. Analytical grade Cobalt (II) nitrate hexahydrate (Sigma-Aldrich), Sodium hydroxide (Thermo Fischer Scientific), and Potassium tetrabromoaurate (III) hydrate (Sigma Aldrich) were used as received from the suppliers without any further purification for sample and electrolyte preparation.

X-ray fluorescence: Data was collected at the XFM beamline at the Australian Synchrotron[2] using a 3 element Vortex energy dispersive SDD array oriented at 90 degrees to the beam in the horizontal plane, with the sample

mounted at 45 degrees to the incident beam[2]. The incident energy was 7680 eV to efficiently excite both Co K and Au M lines, and the beam was focused to a ca. 2 μm spot with a Kirkpatrick-Baez mirror pair. The sample was bidirectionally raster scanned continuously in the 45-degree horizontal plane at a velocity of 50 μms^{-1} with a sampling interval of 2 μm in both the horizontal and vertical direction. The effective dwell per pixel was 40 ms. Fluorescent photons were collected in event mode and the resulting data stream deconvolved into elemental maps using GeoPIXE [3] and exported as 32-bit TIFF images.

s

X-ray absorption near edge spectroscopy (XANES) mapping: Data was collected under the same conditions as fluorescence data with the incident energy stepped over 72 non-uniformly spaced energies from 7680 to 7850 eV between scans. The total scan time per XANES dataset was approximately 70 min. For each energy scan, the Co elemental map was exported as a 32-bit TIFF. Each pixel of the image stack was normalised for $E < 7700$ eV and $E > 7860$ eV. Due to the relatively low signal to noise ratio, the integral edge method[4, 5] was used to determine the change in oxidation state at a per-pixel level with $\mu_1 = 0.15$, $\mu_2 = 1.0$, $E_1 = 7700$ eV, and $E_2 = 7730$ eV[4] with the edge energy reported where the data reaches a normalised intensity of 0.5.

X-ray diffraction (XRD) mapping: Data was collected with an EIGER2 X 1M (Dectris Ltd) photon counting detector [6] placed ca. 6 cm downstream of the sample plane with a Pb beamstop blocking the direct beam. The energy was set to 7680 eV to eliminate the Co fluorescence background. Data was collected similarly to fluorescence data, however, to ensure sufficient diffracted signal was collected; the scan speed was lowered to 5 μms^{-1}. With a sampling interval of 2 μm in both the horizontal and vertical direction, the effective dwell per-pixel was 200 ms. Data was collected in free-run mode[7] with the acquisition time set to 200 ms to match the per-pixel dwell. The total scan time for each XRD map was approximately 6 min.

All diffraction data was processed using Python. Diffraction images were exported as 32-bit TIFFs. The TIFF images were processed and converted to 1D integrated plots using the 1D azimuthal integration function in the pyFAI library in Python calibrated from Co oxide reference data. A mask was applied to the diffraction images to mask the data across the beam stop and the gap area of the detector where the photon counts were zero. The 1D integrated plots showed q values in nm^{-1} in the X axis and intensity/photon counts in the Y axis. Forward scatter leads to some background noise due to the close camera position. Diffraction peaks were clearly visible in the plots (Fig 2c). Gaussian fitting of specific peaks in the background subtracted 1D plots returned values for the peak positions, full width at half maxima (FWHM) and intensities of the peaks. Normalised peak intensity was mapped by integrating integrated intensity of specific peaks at each pixel position in the film before normalising each film to a maximum of one by dividing by the maximum pixel intensity in that map. For the average integrated intensity maps of Au in CoAu films (Fig. 2d,e), the intensity values were again averaged between Au (111) and (200) peaks' average integrated intensity values. The crystal size was calculated for each pixel position from the FWHM after fitting the peaks using the Scherrer equation[8], with the mean and standard deviation for all peaks over all of the pixel positions in each film reported, together with the standard deviation.

Two maps of standard deviation in intensity of the Au (111) and Au (200) peaks observed in the CoAu films were created (Fig. 2 f, g).[9] A 2D azimuthal regrouping was performed individually on each diffraction frame collected for a particular film. The 2D integration returned an unfolded image (if plotted) for the original

diffraction image where the rings appeared as straight lines. All such 2D integrated data were saved as NumPy arrays. The standard deviation in the intensity along the line of the ring in the 2D integrated image (the peak of interest) was calculated using the index of the peak position from previously performed Gaussian fitting and the previously saved NumPy array of the 2D integration. A data frame of standard deviation in intensity for the peak of interest was generated for all frames of the film and a map was created following the same method as the average integrated intensity and crystal size distribution maps.

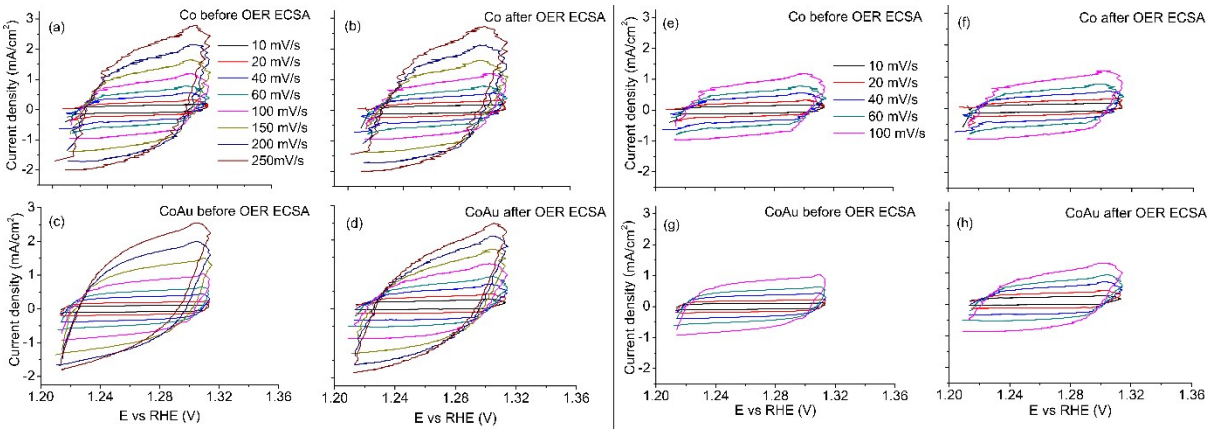

Figure S1: (a)-(d) Cyclic voltammograms (CV) recorded for $Co(OH)_2$ (denoted as Co) and Co(OH)-Au (denoted as CoAu) films in 0.1 M NaOH at various scan rates in the double layer charging region before and after the OER. Here, the CVs measured for ECSA determination are shown for (a) Co before OER, (b) Co after OER, (c) CoAu before OER and (d) CoAu after OER. The surface area was determined from the slopes of the plots in (e)-(f) which are from the cyclic voltammograms (a)-(d) in the range of 10-100 mV s^{-1} scan rates that maintained linearity. Here, (e) Co before OER, (f) Co after OER, (g) CoAu before OER and (h) CoAu after OER are the CVs selected for the ECSA calculations from the recorded CVs shown in (a)-(d) within the range of scan rates 10-100 mV s^{-1} as they maintained linearity and did not show any ohmic behaviour. The slopes and the Electrochemical Surface Area (ECSA) are given below in table S1.

The electrochemically active surface area was calculated by assuming that a flat surface has a specific capacitance of 40 μFcm^{-2} for $Co(OH)_2$.[10]

Table S1. Electrochemically active surface area of Co and CoAu thin films.

Sample	**Slope (mF cm^{-2})**	**Electrochemically Active Surface Area (ECSA) (cm^2)**
$Co(OH)_2$ before OER	8.848	221.2
$Co(OH)_2$ after OER	8.876	221.9
Au-$Co(OH)_2$ before OER	8.0	200.0
Au-$Co(OH)_2$ after OER	9.128	228.2

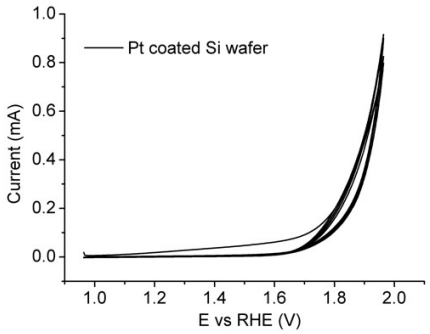

Figure S2: The cyclic voltammogram of Pt coated Si wafer in 0.1M NaOH shows no OER activity in the scan range of 1-1.8 V vs RHE, hence the Pt/Si layer does not influence the OER performance of the films prepared on the Pt coated Si_3N_4 windows used for the synchrotron experiments.

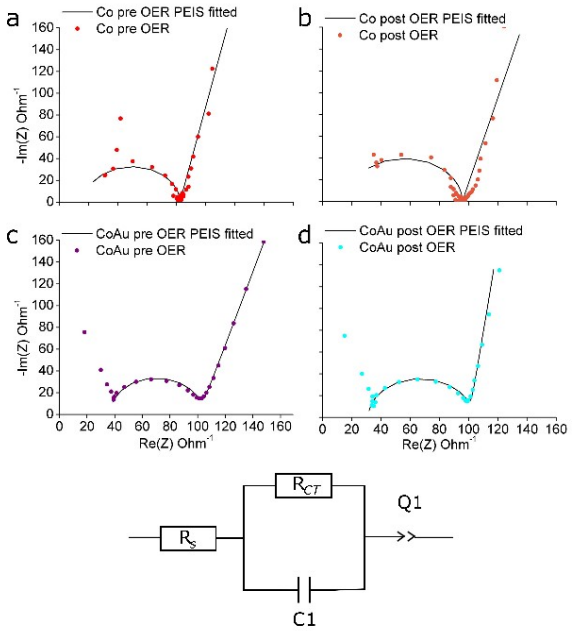

Figure S3: Equivalent circuit and data fitting of Potentio Electrochemical Impedance Spectroscopy (PEIS) of the Co and CoAu films.

The charge transfer resistance (R_{ct}) was determined from fitting the PEIS plots in Figure S3 (a)-(d) which is given below in table S2.

Table S2: Charge transfer resistance (R_{ct}) of Co and CoAu thin films.

Sample	**R_{ct} (Ohm)**
$Co(OH)_2$ before OER	63.94
$Co(OH)_2$ after OER	78.98
Au-$Co(OH)_2$ before OER	64.88
Au-$Co(OH)_2$ after OER	69.11

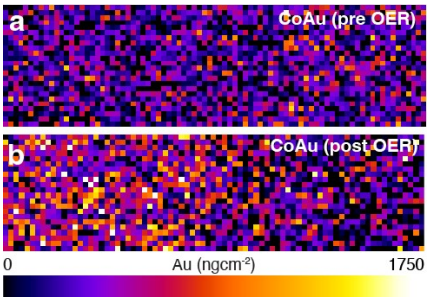

Figure S4: Elemental Au distribution in the CoAu films pre (a) and post (b) OER showing an increase in elemental Au in the post OER sample.

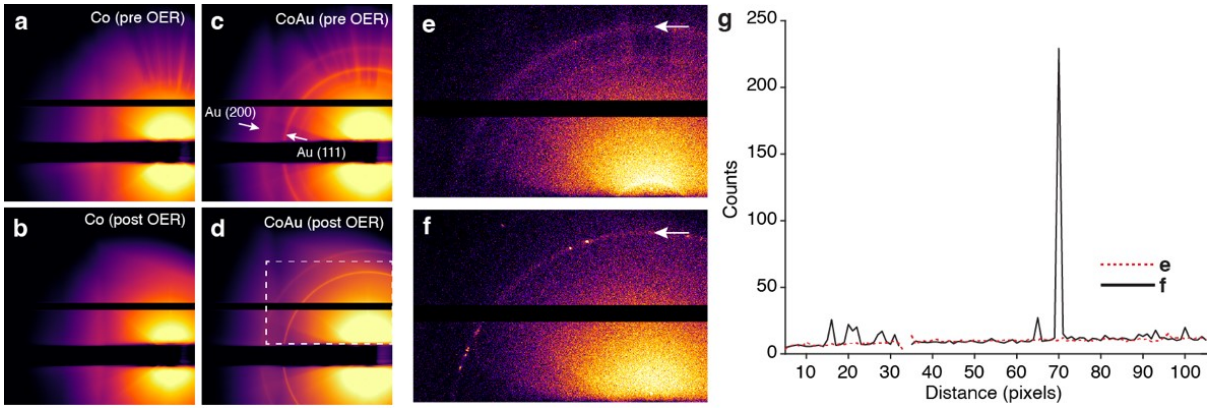

Figure S5: Integrated diffraction patterns of Co (a, b) and CoAu (c, d) pre and post OER respectively. (e, f) show individual images from the CoAu pre and post OER scans with low (e) and high (f) standard deviations in the Au (111) diffraction ring. The diffraction spots are clearly visible in (f). (g) shows plots of the counts azimuthally around the ring indicated with the arrow in (e, f) from the region in the white dashed box in (d). The standard deviation of the plotted data in (g) was used to map the crystal textures in Fig 2(h, i).

References

1. R. Kamar, R. Agoston, G. A. van Riessen, G. Hinsley, A. P. O'Mullane and M. W. Jones, *Journal of Materials Chemistry A*, 2023, **11**, 20816-20823.
2. D. L. Howard, M. D. de Jonge, N. Afshar, C. G. Ryan, R. Kirkham, J. Reinhardt, C. M. Kewish, J. McKinlay, A. Walsh, J. Divitcos, N. Basten, L. Adamson, T. Fiala, L. Sammut and D. J. Paterson, *Journal of Synchrotron Radiation*, 2020, **27**, 1447-1458.
3. C. G. Ryan and D. N. Jamieson, *Nuclear Instruments and Methods in Physics Research B*, 1993, **77**, 203-214.
4. H. Dau, P. Liebisch and M. Haumann, *Analytical and Bioanalytical Chemistry*, 2003, **376**, 562-583.

5. C. Pasquini, S. Liu, P. Chernev, D. Gonzalez-Flores, M. R. Mohammadi, P. Kubella, S. Jiang, S. Loos, K. Klingan, V. Sikolenko, S. Mebs, M. Haumann, P. Beyer, L. D'Amario, R. D. L. Smith, I. Zaharieva and H. Dau, *Analytical and Bioanalytical Chemistry*, 2021, **413**, 5395-5408.
6. T. Donath, D. Sisak Jung, M. Burian, V. Radicci, P. Zambon, A. N. Fitch, C. Dejoie, B. Zhang, M. Ruat, M. Hanfland, C. M. Kewish, G. A. van Riessen, D. Naumenko, H. Amenitsch, G. Bourenkov, G. Bricogne, A. Chari and C. Schulze-Briese, *Journal of Synchrotron Radiation*, 2023, **30**, 723-738.
7. M. W. M. Jones, G. A. van Riessen, N. W. Phillips, C. E. Schrank, G. N. Hinsley, N. Afshar, J. Reinhardt, M. D. de Jonge and C. M. Kewish, *J Synchrotron Radiat*, 2022, **29**, 480-487.
8. F. T. L. Muniz, M. R. Miranda, C. Morilla dos Santos and J. M. Sasaki, *Acta Crystallographica Section A: Foundations and Advances*, 2016, **72**, 385-390.
9. P. Gueriau, S. Réguer, N. Leclercq, C. Cupello, P. M. Brito, C. Jauvion, S. Morel, S. Charbonnier, D. Thiaudière and C. Mocuta, *Journal of The Royal Society Interface*, 2020, **17**, 20200216.
10. H. Deng, C. Zhang, Y. Xie, T. Tumlin, L. Giri, S. P. Karna and J. Lin, *Journal of Materials Chemistry A*, 2016, **4**, 6824-6830.